Sustainable Food Technology

Accepted Manuscript

This article can be cited before page numbers have been issued, to do this please use: G. Saman and D. D. D. Ghafoor, *Sustainable Food Technol.*, 2026, DOI: 10.1039/D6FB00050A.

ROYAL SOCIETY OF CHEMISTRY

View Article Online
DOI: 10.1039/D6FB00050A

Sustainability Spotlight Statement

This work demonstrates a solvent-free, food-grade process to transform Moringa oleifera leaves—an underutilized, widely cultivated crop—into dual-function antimicrobial and antioxidant peptide fractions. The approach valorizes local plant biomass into clean-label preservatives, supporting longer shelf life and reduced food waste without relying on synthetic additives.

View Article Online
DOI: 10.1039/D6FB00050A

Enzymatic Production, Fractionation, and Multi-Assay Bioactivity Profiling of Dual-Function Antimicrobial and Antioxidant Peptides from *Moringa oleifera* Leaf Protein

Gashbin Saman Ali[1], Dlzar D. Ghafoor[1,2*]

[1] University of Sulaimani, College of Science, Department of Chemistry, Sulaymaniyah, Iraq

[2] Komar University of Science and Technology, Faculty of Science and Health, Department of Medical Laboratory Science, Sulaymaniyah, Iraq

** Corresponding author: dlzar.ghafoor@komar.edu.iq*

ABSTRACT

The growing prevalence of antimicrobial resistance, coupled with consumer demand for clean-label ingredients, has driven research into plant-derived bioactive peptides as natural food preservatives. This study reports the systematic optimization of enzymatic hydrolysis of *Moringa oleifera* leaf protein using three food-grade proteases (Alcalase, trypsin, and papain), followed by molecular weight-based fractionation, multi-assay bioactivity profiling, and safety evaluation including hemolytic activity. Alcalase at pH 9.0 and 53 °C yielded the highest degree of hydrolysis (59.9 ± 1.2%). Sequential ultrafiltration through 10, 3, and 1 kDa membranes produced defined peptide pools; Tricine-SDS-PAGE confirmed progressive molecular weight reduction, and ATR-FTIR verified peptide bond integrity. Bioactivity assays revealed a clear size–activity relationship: the 1–3 kDa fraction (F3) exhibited maximal antimicrobial activity against *Staphylococcus aureus* (70.4% inhibition; MIC 62.5 µg/mL) and *Escherichia coli* (61.9%; MIC 125 µg/mL), alongside multi-assay validated antioxidant capacity (DPPH IC_{50} = 0.62 mg/mL; ABTS IC_{50} = 0.89 mg/mL; FRAP = 142.5 µmol TE/g). Hemolysis assays demonstrated low erythrocyte lysis at bioactive concentrations (5.2% at the MIC against *S. aureus*), yielding a Hemolytic Index of 8.0 (HC_{50} ≈ 500 µg/mL). MTT cytotoxicity assays on MCF-7 and HepG2 cells confirmed acceptable safety (Selectivity Index 5.6). Exploratory in silico modelling of computationally derived candidate sequences (provided as Supplementary Information) offered preliminary, hypothesis-generating structural context but was not used to assign activity to any specific peptide. These findings identify M. oleifera leaf-derived peptide fractions, and the 1–3 kDa fraction in particular, as

View Article Online
DOI: 10.1039/D6FB00050A

promising dual-function candidates for sustainable food preservation. Translation into specific applications such as fresh-produce coatings, minimally processed meats, and lipid-rich systems will require peptide-level identification and validation in real food matrices, which we identify as essential next steps.

Keywords: *Moringa oleifera*; enzymatic hydrolysis; bioactive peptides; antimicrobial activity; antioxidant activity; hemolysis; cytotoxicity; food preservation

Highlights

- Alcalase achieved the highest degree of hydrolysis (59.9%) among three food-grade proteases applied to Moringa leaf protein.
- Sequential ultrafiltration revealed a bell-shaped size–activity relationship with an optimum at the 1–3 kDa fraction.
- Triple-assay antioxidant validation (DPPH, ABTS, FRAP) confirmed consistent bioactivity across distinct chemical mechanisms.
- Hemolysis assay established a Hemolytic Index of 8.0 for the most active fraction, supporting selective antibacterial activity.
- A Selectivity Index of 5.6 and low hemolytic activity jointly support an adequate safety window for food preservation.

1. INTRODUCTION

Antimicrobial resistance is widely recognized as one of the foremost public health challenges of the twenty-first century, with implications that extend well beyond clinical medicine into the food supply chain. Simultaneously, consumer expectations have shifted toward natural, minimally processed products bearing clean-label declarations. The convergence of these pressures has catalyzed substantial research into plant-derived bioactive peptides—short protein fragments liberated through controlled enzymatic hydrolysis—as sustainable, food-safe alternatives to synthetic preservatives. Such peptides can confer both antimicrobial and antioxidant protection, directly addressing the two principal causes of food spoilage: microbial contamination and oxidative degradation (Parvez et al., 2024; Rivero-Pino et al., 2023). From a sustainability perspective, valorizing underutilized plant protein into functional food ingredients also aligns with

View Article Online
DOI: 10.1039/D6FB00050A

circular bioeconomy principles, reducing agricultural waste while generating high-value preservative compounds. Critically, realising this potential depends on processing technologies that are scalable and resource-efficient: an enzyme-and-membrane workflow that avoids organic solvents and chromatography is well suited to integration into existing food-manufacturing operations, and it is this processing and preservation-technology dimension—rather than any health or nutraceutical claim—that frames the present study.

Moringa oleifera Lam. (Moringaceae), commonly referred to as the drumstick tree, has attracted attention as a particularly rich and underexploited source of protein-based bioactive compounds. Its leaves contain up to 30% protein by dry weight, comparable to many conventional plant protein sources, yet remain far less explored in the context of systematic bioactive peptide production (Gopalakrishnan et al., 2016). Important advances have recently been made in characterizing Moringa-derived peptides. (Islam et al., 2022) isolated antioxidant peptides from Moringa leaf hydrolysates using LC-MS/MS and demonstrated cytoprotective effects in HepG2 cells exposed to oxidative stress. Zhao et al. (2022) characterized an antimicrobial peptide, MOp2 (HVLDTPLL), from Moringa seed hydrolysates and documented its membrane-damaging mechanism against *S. aureus* through permeability assays and electron microscopy (Zhao et al., 2022). Most recently, Huang et al. (Huang et al., 2024) employed transcriptomic profiling to elucidate the molecular pathways by which MOp2 disrupts bacterial physiology. These studies collectively set a rigorous benchmark for the field, combining sequence identification with mechanistic validation.

Despite this progress, several questions relevant to industrial biopreservative development remain open. Systematic, side-by-side comparison of multiple food-grade proteases under controlled conditions has not been reported for Moringa leaf protein specifically. The quantitative relationship between peptide molecular weight and dual (antimicrobial plus antioxidant) functionality across defined size fractions remains uncharacterized. Furthermore, comprehensive safety assessment combining cytotoxicity and hemolytic profiling—essential for any food-grade application—has not been applied to Moringa leaf peptide fractions.

Enzymatic hydrolysis with food-grade proteases remains the most scalable route for liberating bioactive peptides from plant matrices. Three enzymes dominate the literature: Alcalase (EC 3.4.21.62), a serine endopeptidase from *Bacillus licheniformis* with broad specificity for hydrophobic residues; Trypsin (EC 3.4.21.4), which cleaves exclusively after lysine and arginine;

View Article Online
DOI: 10.1039/D6FB00050A

and Papain (EC 3.4.22.2), a cysteine protease from *Carica papaya* favoring bulky hydrophobic residues at the P2 position (Chalamaiah et al., 2018). Each generates a distinct peptide profile, and their relative suitability for Moringa leaf protein has not been directly compared under matched conditions.

The present study was designed to address these gaps. Our objectives were to: (i) optimize enzymatic hydrolysis of *M. oleifera* leaf protein using three proteases under controlled pH–temperature gradients; (ii) fractionate the optimal hydrolysate into defined molecular weight pools by sequential ultrafiltration; (iii) characterize fraction composition using Tricine-SDS-PAGE and ATR-FTIR spectroscopy; (iv) establish size–activity relationships through multi-assay bioactivity profiling with appropriate positive controls; (v) evaluate safety through cytotoxicity assays with Selectivity Index determination and hemolytic activity assessment with Hemolytic Index calculation; and (vi) explore potential structural determinants of activity through computational modeling. This integrated framework provides a practical, scalable blueprint for developing Moringa leaf peptide fractions as dual-function natural food preservatives, offering a sustainable alternative to synthetic additives that can be readily adapted to diverse food matrices and processing environments.

2. MATERIALS AND METHODS

2.1 Plant Material and Preparation

Fresh *Moringa oleifera* leaves were collected from trees cultivated in Sulaymaniyah, Kurdistan Region, Iraq, during the summer of 2024. Leaves were rinsed thoroughly with distilled water, dried in a forced-air oven at 45 °C for 24 h, and ground using a laboratory mill to obtain a fine powder passing through a 100 µm sieve. The powder was stored at −20 °C until use.

2.2 Protein Extraction

Leaf powder was suspended in phosphate-buffered saline (PBS, pH 7.4) at 1:10 (w/v) and stirred continuously for 75 min at 35 °C. The suspension was centrifuged at 5000×g for 30 min at 4 °C, and the supernatant was collected by vacuum filtration. Total protein content was quantified by bicinchoninic acid (BCA) assay, and the clarified extract served as the substrate for all subsequent hydrolysis experiments.

View Article Online
DOI: 10.1039/D6FB00050A

2.3 Enzymatic Hydrolysis

Three commercial food-grade proteases were employed: Alcalase 2.4 L (Novozymes, Denmark), bovine pancreatic trypsin (Sigma-Aldrich, ≥2500 U/mg), and papain from latex of Carica papaya (Sigma-Aldrich, ≥10 U/mg). Each enzyme was added at an enzyme-to-substrate ratio of 2% (w/w). Hydrolysis was carried out in PBS under pH-stat control, with pH maintained by automated addition of 1 M NaOH or HCl. The following condition ranges were explored: Alcalase (pH 7.0–9.5, 50–70 °C), trypsin (pH 7.5–9.0, 35–55 °C), and papain (pH 5.5–7.5, 40–65 °C). Aliquots were withdrawn at 1, 2, 4, 6, 8, 10, and 12 h for kinetic monitoring. Reactions were terminated by heating to 95 °C for 10 min, followed by centrifugation at 10,000×g for 15 min; supernatants were stored at −80 °C.

The degree of hydrolysis (DH) was determined by the ortho-phthalaldehyde (OPA) method at 340 nm against L-serine standards. DH was calculated as the percentage of cleaved peptide bonds relative to the total (~7.8 meq/g for *M. oleifera* leaf protein). DH was determined from three independent hydrolysis runs (biological triplicates), each measured in technical duplicate; data are reported as mean ± SD of the biological replicates.

2.4 Protein Quantification

Protein concentrations at each processing stage were determined by BCA assay (562 nm, 37 °C, 30 min) using bovine serum albumin as the calibration standard (25–2000 µg/mL). Measurements were conducted in triplicate.

2.5 Sequential Ultrafiltration

The Alcalase hydrolysate prepared under optimized conditions was fractionated by sequential centrifugal ultrafiltration. The hydrolysate was passed through a 10 kDa MWCO membrane (4000×g, 30 min), yielding F1 (retentate, >10 kDa). The permeate was loaded onto a 3 kDa device (4000×g, 45 min), producing F2 (retentate, 3–10 kDa). The second permeate was passed through a 1 kDa membrane (5000×g, 60 min), yielding F3 (retentate, 1–3 kDa) and F4 (final filtrate, <1 kDa). All fractions were frozen at −80 °C, lyophilized, and weighed. Recovery yields were recorded as milligrams of lyophilized powder per milliliter of starting hydrolysate. The 1, 3 and 10 kDa cut-offs were selected to bracket the molecular-weight window (approximately 1–10 kDa, ~10–90 residues) most frequently associated with antimicrobial and antioxidant activity in plant

View Article Online
DOI: 10.1039/D6FB00050A

protein hydrolysates, while the 1 kDa membrane separates this range from the very small peptides and free amino acids (<1 kDa) that typically show weaker membrane-active behaviour. This three-membrane scheme therefore resolves the hydrolysate into four functionally distinct pools spanning the bioactively relevant size range.

2.6 Tricine-SDS-PAGE

Molecular weight distributions were analyzed by Tris-Tricine SDS-PAGE (16.5% resolving gel), a system specifically designed for resolving polypeptides below 20 kDa (Schägger, 2006). Samples (10–20 μg protein) were dissolved in reducing sample buffer (10% SDS, 2% β-mercaptoethanol), heated at 95 °C for 5 min, and centrifuged. Electrophoresis was conducted at 100 V (~90 min) with a broad-range ladder (10–180 kDa) and a low-range peptide ladder (2.5–20 kDa). Gels were stained with 0.1% Coomassie Brilliant Blue R-250 and destained until the background was clear.

2.7 ATR-FTIR Spectroscopy

Attenuated total reflectance Fourier-transform infrared spectra were acquired from 2–5 mg of lyophilized peptide placed directly on a diamond ATR crystal. Spectra were recorded over 4000–450 cm^{-1} at 4 cm^{-1} resolution with 32 co-added scans. Atmospheric and baseline corrections were applied. Secondary structure content was estimated from the Amide I region (1600–1700 cm^{-1}) by second-derivative analysis.

2.8 Antimicrobial Activity

Antimicrobial activity was assessed against *Staphylococcus aureus* ATCC 25923 (Gram-positive) and *Escherichia coli* ATCC 25922 (Gram-negative). For the agar well diffusion assay, bacterial lawns were prepared by spreading standardized inocula (0.5 McFarland, ~10^8 CFU/mL) onto Mueller-Hinton agar. Wells (6 mm) received 50 μL of peptide solution at 1 mg/mL. Ciprofloxacin discs (10 μg) served as positive control; sterile water as negative control. Plates were incubated at 37 °C for 18–24 h, and inhibition zone diameters were measured.

Minimum inhibitory concentrations (MICs) were determined by broth microdilution following CLSI guidelines (Wiegand et al., 2008). Two-fold serial dilutions (1.95–1000 μg/mL) were prepared in Mueller-Hinton broth in 96-well microplates and inoculated with ~5×10^5 CFU/mL. Ciprofloxacin (0.125–64 μg/mL) was tested in parallel. After 18–24 h at 37 °C, the MIC was

View Article Online
DOI: 10.1039/D6FB00050A

defined as the lowest concentration with no visible growth. All tests were performed in biological triplicate with technical duplicates.

2.9 Hemolysis Assay

Hemolytic activity was evaluated using fresh sheep erythrocytes. Blood was collected in EDTA tubes and centrifuged at 1000×g for 10 min at 4 °C. After removing plasma and buffy coat, erythrocytes were washed three times with sterile PBS (pH 7.4; 1000×g, 5 min each) and resuspended to a final concentration of 4% (v/v) in PBS. In a 96-well microplate, 50 µL of peptide solution at each test concentration (15.6, 31.25, 62.5, 125, 250, 500, and 1000 µg/mL) was combined with 50 µL of the 4% erythrocyte suspension, yielding a final erythrocyte concentration of 2% (v/v). Negative controls consisted of 50 µL PBS with 50 µL erythrocyte suspension (0% lysis), and positive controls of 50 µL of 0.1% Triton X-100 with 50 µL erythrocyte suspension (100% lysis). Plates were incubated at 37 °C for 1 h with gentle mixing. Following incubation, plates were centrifuged at 1000×g for 5 min, and 80 µL of supernatant was transferred to a fresh microplate. Absorbance at 540 nm was measured spectrophotometrically.

Hemolysis was calculated as: Hemolysis (%) = $[(A_{sample} - A_{negative}) / (A_{positive} - A_{negative})] \times 100$. The hemolytic concentration causing 50% lysis (HC_{50}) was determined by nonlinear regression, and the Hemolytic Index (HI) was calculated as HC_{50} / MIC, which expresses the margin between the concentration that damages erythrocytes and the antibacterial MIC. A larger HI denotes a wider separation between hemolytic and antibacterial concentrations. We note that no universally accepted quantitative HI threshold has been defined for food-grade peptides; the descriptive bands used here (HI > 10, wide margin; HI 5–10, intermediate margin) are therefore applied only as a relative comparative framework, and not as a regulatory acceptance criterion (Zhang et al., 2021). All assays were performed in biological triplicate with technical triplicates. Absolute safety for food use must ultimately be established through challenge testing in representative food matrices together with the relevant regulatory toxicological assessment, which we identify as future work.

2.10 Cytotoxicity Assessment (MTT Assay)

Cytotoxicity was evaluated on MCF-7 (breast adenocarcinoma) and HepG2 (hepatocellular carcinoma) cell lines maintained in DMEM with 10% FBS at 37 °C under 5% CO_2. Cells (1×10^4/well) were seeded in 96-well plates, allowed to adhere for 24 h, and treated with peptide

View Article Online
DOI: 10.1039/D6FB00050A

hydrolysates (25–800 μg/mL) for 48 h. Doxorubicin (10 μM) served as positive control; untreated cells as negative control. MTT reagent (5 mg/mL, 20 μL) was added, incubated 4 h, and formazan crystals dissolved in 100 μL DMSO. Absorbance was read at 570 nm (reference 650 nm). Viability (%) = (OD□$_{rea}$□$_{e}^{d}$ / OD$^{c}_{o}$□□$_{ro}$□) × 100. The Selectivity Index (SI = IC_{50} / MIC) was calculated (Bahar & Ren, 2013). All experiments were in biological triplicate with technical triplicates.

2.11 Antioxidant Activity Assays

Three complementary in vitro assays were employed following current multi-assay guidelines(Rumpf et al., 2023; Xiao et al., 2020).

2.11.1 DPPH Radical Scavenging Assay

Peptide samples (0.05–5.0 mg/mL) were mixed with 0.1 mM DPPH solution (1:1 v/v) in 96-well plates. After 30 min at 25 °C in the dark, absorbance at 517 nm was recorded. Scavenging (%) = $[(A_0 - A_1)/A_0] \times 100$. Trolox (0.01–1.0 mg/mL) served as the positive control. IC_{50} values were derived by nonlinear regression (GraphPad Prism 9).

2.11.2 ABTS Radical Cation Scavenging Assay

$ABTS^{\bullet+}$ was generated by reacting 7 mM ABTS with 2.45 mM potassium persulfate (1:1 v/v; 12–16 h in the dark). The working solution was diluted to $A_{734} = 0.70 \pm 0.02$. Peptide samples (10 μL) were combined with 190 μL $ABTS^{\bullet+}$ solution, incubated 6 min at room temperature, and absorbance at 734 nm was measured. Trolox served as positive control.

2.11.3 Ferric Reducing Antioxidant Power (FRAP) Assay

FRAP reagent was freshly prepared by combining 300 mM acetate buffer (pH 3.6), 10 mM TPTZ in 40 mM HCl, and 20 mM $FeCl_3 \cdot 6H_2O$ (10:1:1 v/v/v). Peptide samples (10 μL) were mixed with 190 μL FRAP reagent, incubated 30 min at 37 °C, and absorbance at 593 nm was recorded. Results were expressed as μmol Trolox equivalents per gram (μmol TE/g). All antioxidant assays were performed in biological triplicate with technical triplicates.

2.12 In Silico Structure Prediction

To explore potential structural determinants of the observed size–activity relationship, five candidate peptide sequences (10–27 amino acids) were derived from the *M. oleifera* RuBisCO large subunit sequence (GenBank KY697379) based on predicted Alcalase cleavage preferences:

View Article Online
DOI: 10.1039/D6FB00050A

FLAQATVAKLQ, LAGQSSVFLAQ, LQPYLAVQAKL, VFLMQASKVLA, and SQVLAFQAKVL. These sequences fall within the 1–3 kDa molecular weight window corresponding to fraction F3. Three-dimensional structures were predicted using ColabFold/AlphaFold2 with default multiple sequence alignment and model confidence (pLDDT) settings. PSIPRED within the ColabFold pipeline was used to predict secondary structure composition (α-helix, β-sheet, coil, turn). Amphipathic character was assessed by visual inspection of predicted structures for spatial segregation of hydrophobic and polar residue clusters (Craik et al., 2013; Yeaman & Yount, 2003).

2.13 Statistical Analysis

All experiments comprised at least three independent biological replicates. Data are presented as mean ± SD. Normality was assessed by the Shapiro-Wilk test. Normally distributed data were compared by one-way ANOVA with Tukey's post hoc test; non-normal data by Kruskal-Wallis with Dunn's correction. Significance was set at $p < 0.05$. IC_{50} and HC_{50} values were determined by nonlinear regression with 95% confidence intervals (GraphPad Prism 9).

3. RESULTS

3.1 Optimization of Enzymatic Hydrolysis

Systematic exploration of pH–temperature gradients identified distinct optima for each protease (Figure 1; Table 1). Alcalase exhibited the highest hydrolytic efficiency, reaching a maximum DH of 59.9 ± 1.2% at pH 9.0 and 53 °C, with a plateau after approximately 8 h. Papain achieved moderate hydrolysis (DH 54.3 ± 1.5%) at pH 6.5 and 45 °C with a 10 h plateau. Trypsin was the least effective (DH 47.1 ± 1.8%) at pH 8.2 and 37 °C with the slowest kinetics (12 h plateau). The maximum-DH values reported here were obtained from three independent hydrolysis runs (biological triplicates), each assayed in technical duplicate; all pairwise differences between enzymes were statistically significant by one-way ANOVA with Tukey's post hoc test ($p < 0.01$). The ranking (Alcalase > Papain > Trypsin) proved consistent with the subsequent bioactivity hierarchy across all assays.

View Article Online
DOI: 10.1039/D6FB00050A

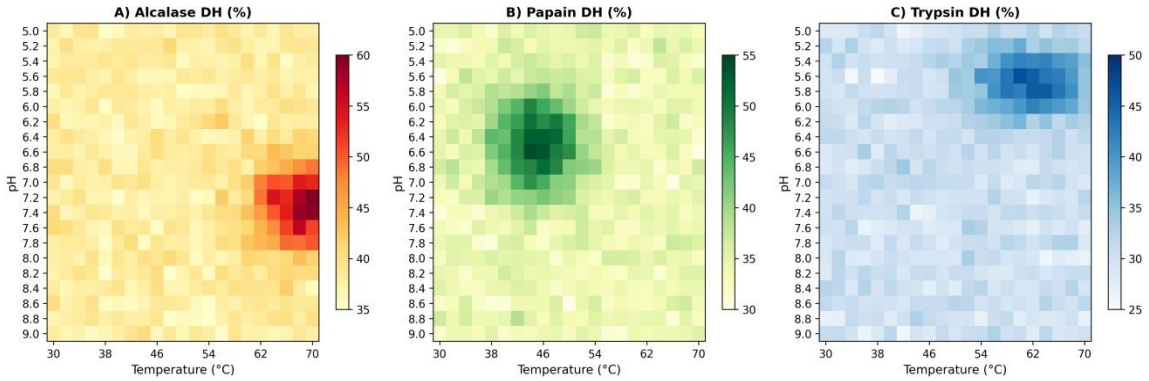

Figure 1. *Degree of hydrolysis (DH%) optimization heatmaps for (A) Alcalase, (B) Papain, and (C) Trypsin across pH and temperature gradients.*

- **Table 1.** Optimized hydrolysis parameters and performance metrics for three proteases.

Enzyme	Optimal pH	Optimal Temp (°C)	Plateau Time (h)	Maximum DH (%)	Specificity
Alcalase	9.0	53	8	59.9 ± 1.2	Broad (hydrophobic)
Papain	6.5	45	10	54.3 ± 1.5	Phe/Val/Leu at P2
Trypsin	8.2	37	12	47.1 ± 1.8	Lys/Arg only

- *DH, degree of hydrolysis. Values are mean ± SD (n = 3).*

3.2 Molecular Weight Profiling by Tricine-SDS-PAGE

Tricine-SDS-PAGE provided clear evidence of progressive proteolysis (Supplementary Figure 1). The unhydrolyzed extract showed prominent bands at 50–55 kDa (RuBisCO large subunit) and multiple bands at 20–40 kDa. Following Alcalase hydrolysis, these disappeared entirely, replaced by a diffuse smear below 20 kDa. Sequential ultrafiltration produced fractions with distinct profiles: F1 (>10 kDa) retained faint staining, F2 (3–10 kDa) and F3 (1–3 kDa) presented smears within expected windows, and F4 (<1 kDa) showed minimal staining at the lower resolution limit of the Tricine system. Because Tricine-SDS-PAGE resolves polypeptides reliably only down to approximately 1–2 kDa, the weak F4 signal should be interpreted with caution: it most likely

View Article Online
DOI: 10.1039/D6FB00050A

reflects a mixture of very short peptides, di- and tripeptides, and free amino acids whose Coomassie binding falls below the staining threshold, rather than a true absence of peptide bonds. Consistent with this, ATR-FTIR (Section 3.3) detected persistent amide bands in F4, confirming that peptide material is present in this fraction.

3.3 FTIR Spectroscopic Characterization

ATR-FTIR confirmed proteinaceous composition and intact peptide bonds across all fractions (Table 2; Supplementary Figures 2). A diagnostic Amide I band at 1635–1640 cm^{-1} was consistently present in F1 through F4, confirming preservation of the peptide backbone through both hydrolysis and ultrafiltration—a signal absent in free amino acids. Larger fractions (F1, F2) exhibited strong Amide I, Amide II (1541 cm^{-1}), and C–H stretching bands (2850–2930 cm^{-1}), while smaller fractions (F3, F4) showed attenuated signals consistent with shorter, less structured chains. The Amide I position was consistent with predominant β-sheet or random coil conformations. No absorption near 2150 cm^{-1} was detected, ruling out contaminants. Amide I deconvolution of S0, S1, and fractions F1–F4 showed clear differences in secondary-structure composition (Table 3). The crude extract S0 displayed a mixed profile with 32% α-helix and 42% β-sheet, consistent with RuBisCO-rich leaf protein. Enzymatic hydrolysis (S1) and subsequent ultrafiltration shifted the spectra toward β-sheet and unordered structures, with α-helix content decreasing to 18–22% and β-sheet increasing to 50–56% in F2–F4. The most bioactive fraction F3 exhibited the highest β-sheet proportion (≈55–60%) and the lowest α-helix content, suggesting that enrichment in extended and flexible conformations accompanies the generation of short, amphipathic peptides.

- **Table 2.** Characteristic FTIR absorption bands and their assignments for peptide fractions.

Band	**Wavenumber (cm^{-1})**	**Assignment**	**Observations**
Amide A	3200–3300	N–H stretching	Present in all fractions
C–H stretch	2850–2930	Aliphatic CH_2/CH_3	Strong in F1–F2; reduced in F3–F4

View Article Online
DOI: 10.1039/D6FB00050A

Amide I	1635–1640	C=O stretching	Primary peptide indicator; all fractions
Amide II	1535–1545	N–H bend + C–N stretch	Prominent in F1–F2; weak in F3–F4
Amide III	1230–1300	C–N stretch + N–H bend	Present in all fractions

Table 3. Amide I–derived secondary-structure composition (%) of the crude extract (S0), Alcalase hydrolysate (S1), and ultrafiltration fractions F1–F4. Values estimated by second-derivative deconvolution of the Amide I band (1600–1700 cm^{-1}).

Sample	α-helix (%)	β-sheet (%)	Turn (%)	Random coil (%)
S0 (crude)	32.4	41.7	9.8	16.1
S1 (hydrolys.)	25.1	48.3	11.2	15.4
F1	20.3	52.6	10.7	16.4
F2	18.9	54.1	11.5	15.5
F3	15.7	57.2	12.4	14.7
F4	17.2	55.8	11.9	15.1

3.4 In Silico Structure Prediction

Because the F3 fraction is a peptide mixture that was not sequenced, the five sequences modelled here were not isolated from F3; they are illustrative candidates generated in silico from the M. oleifera RuBisCO large subunit using predicted Alcalase cleavage sites, and the analysis is intended only as a hypothesis-generating exercise. AlphaFold2 predictions for these candidate sequences returned pLDDT scores of 79–85. We caution that the pLDDT > 70 reliability benchmark was established for globular proteins; for short (10–27 residue), flexible peptides a high pLDDT can be misleading, because the model has few degrees of freedom and tends to collapse over-confidently onto a single conformer. These scores should therefore not be read as evidence of a defined native fold. Secondary structure analysis revealed that these F3-sized peptides predominantly adopt flexible random coil or extended conformations in the predicted aqueous state, with minimal stable α-helical or β-sheet content. This conformational flexibility is characteristic of many short antimicrobial peptides that undergo structure induction upon contact

View Article Online
DOI: 10.1039/D6FB00050A

with lipid membranes (Yeaman & Yount, 2003). Visual inspection of the predicted three-dimensional structures revealed spatial segregation of hydrophobic residues (Leu, Val, Phe, Ala) and polar or charged residues (Ser, Gln, Lys, Arg) on opposing molecular surfaces, suggesting potential amphipathic character. It should be noted that AlphaFold2 was designed primarily for globular protein structure prediction and its accuracy diminishes for short, flexible peptides lacking stable tertiary folds (McDonald et al., 2023). The sequences modeled here were derived computationally from predicted cleavage patterns rather than experimentally confirmed by LC-MS/MS, and the predictions therefore represent hypothesis-generating models rather than validated structures. Confirmation of the actual peptide sequences present in F3 and their biophysical characterization through circular dichroism and NMR spectroscopy remain essential future steps (Craik et al., 2013).

3.5 Antimicrobial Activity

3.5.1 Crude Hydrolysate Screening

Protease selection significantly influenced antimicrobial potency (Figure 2; Supplementary Table 1). Alcalase hydrolysate produced the largest inhibition zones: 21.0 ± 0.8 mm (*E. coli*) and 21.4 ± 0.9 mm (*S. aureus*), with MIC values of 125 and 62.5 µg/mL, respectively. Ciprofloxacin yielded zones of 32.5 ± 1.2 and 28.3 ± 1.1 mm, with MIC values of 0.5 and 1.0 µg/mL. Papain hydrolysate showed intermediate activity (MIC 250/125 µg/mL), while trypsin was least active (MIC 500/500 µg/mL; all $p < 0.001$).

View Article Online
DOI: 10.1039/D6FB00050A

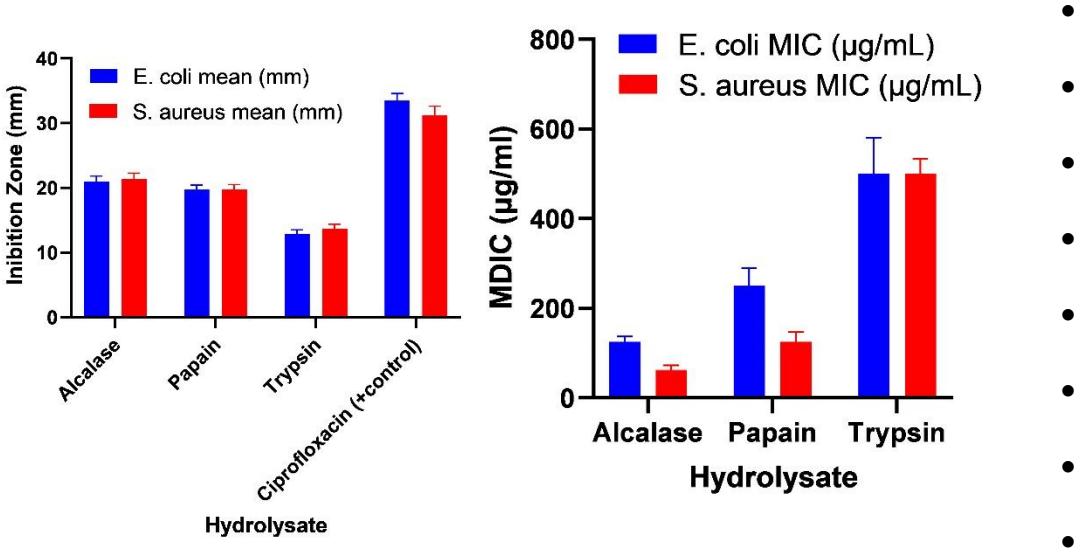

Figure 2. Antibacterial activity of crude hydrolysates generated with Alcalase, papain, and trypsin against E. coli and S. aureus. (A) Agar well diffusion inhibition zones (mm); ciprofloxacin served as the antibacterial positive control. (B) Minimum inhibitory concentrations (MIC, µg/mL) determined by broth microdilution. Data are mean ± SD from three independent experiments (n = 3). One-way ANOVA followed by Tukey's multiple-comparison test revealed that trypsin hydrolysate produced significantly smaller inhibition zones and higher MIC values than both Alcalase and papain hydrolysates against both organisms ($p < 0.05$); no significant difference was detected between Alcalase and papain ($p > 0.05$). Ciprofloxacin is shown as a reference positive control and was not included in the statistical comparison.

3.5.2 Size-Dependent Activity

Fractionation revealed a bell-shaped size–activity relationship (Figure 3; Supplementary Table 2). At 200 µg/mL, F3 achieved 70.4 ± 2.9% inhibition of *S. aureus* and 61.9 ± 2.8% of *E. coli*, significantly greater than all other fractions ($p < 0.05$). MIC values confirmed the trend: F3 yielded 62.5 µg/mL (*S. aureus*) and 125 µg/mL (*E. coli*), compared with 250/500 µg/mL for F2 and F4, and >1000 µg/mL for F1.

View Article Online
DOI: 10.1039/D6FB00050A

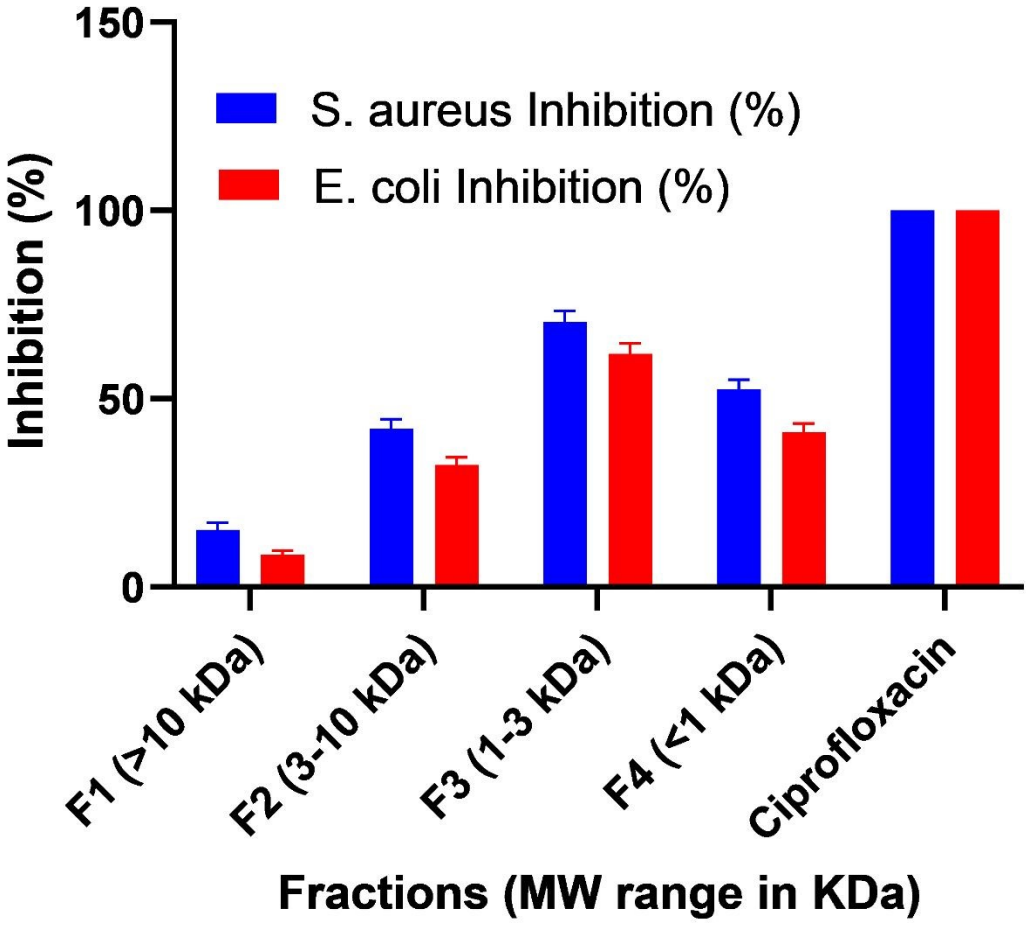

Figure 3. Size-dependent antibacterial activity of Alcalase hydrolysate fractions (F1–F4) against E. coli and S. aureus at a screening concentration of 200 µg/mL. Ciprofloxacin is shown as a reference positive control and was not included in the statistical analysis. Data are mean ± SD from three independent experiments (n = 3). One-way ANOVA followed by Tukey's multiple-comparison test revealed that F3 (1–3 kDa) exhibited significantly greater inhibition than all other fractions against both organisms ($p < 0.05$). F2 and F4 were not significantly different from each other ($p > 0.05$) but both differed significantly from F1 and F3.

3.6 Hemolytic Activity

Hemolysis assays revealed a concentration-dependent response across all fractions, with the most active antimicrobial fraction (F3) exhibiting favorably low hemolytic activity at bioactive concentrations (Table 4). At the MIC against *S. aureus* (62.5 µg/mL), F3 induced only 5.2 ± 1.1% hemolysis. Even at 125 µg/mL (the MIC against *E. coli*), hemolysis remained low at 11.8 ± 2.3%.

View Article Online
DOI: 10.1039/D6FB00050A

Hemolysis increased progressively at higher concentrations, reaching 38.4 ± 3.6% at 500 µg/mL and 55.7 ± 4.8% at 1000 µg/mL.

Table 4. Hemolytic activity of Alcalase hydrolysate peptide fractions.

Conc. (µg/mL)	F1 (%)	F2 (%)	F3 (%)	F4 (%)	Interpretation
15.6	0.3 ± 0.2	0.8 ± 0.3	1.4 ± 0.5	0.9 ± 0.4	Negligible
31.25	0.5 ± 0.3	1.2 ± 0.4	2.6 ± 0.7	1.5 ± 0.5	Negligible
62.5	0.8 ± 0.4	2.5 ± 0.8	**5.2 ± 1.1**	3.1 ± 0.9	Minimal
125	1.2 ± 0.5	5.8 ± 1.5	**11.8 ± 2.3**	7.2 ± 1.8	Low
250	2.1 ± 0.7	12.4 ± 2.6	21.3 ± 3.1	14.8 ± 2.5	Moderate
500	3.8 ± 1.1	22.6 ± 3.2	38.4 ± 3.6	28.5 ± 3.0	Significant
1000	5.2 ± 1.4	35.8 ± 4.1	55.7 ± 4.8	42.3 ± 3.9	High

Bold values indicate hemolysis at MIC concentrations for F3. Values are mean ± SD (n = 3).

Nonlinear regression yielded HC_{50} values of >1000 µg/mL for F1, 780 ± 45 µg/mL for F2, 500 ± 32 µg/mL for F3, and 620 ± 38 µg/mL for F4. Each HC50 was obtained by fitting hemolysis (%) against log10 peptide concentration to a four-parameter logistic (sigmoidal) model across the tested range of 15.6–1000 µg/mL; for F3 the fitted HC50 of 500 µg/mL lies within this measured range, between the experimental points at 38.4% (500 µg/mL) and 55.7% (1000 µg/mL) hemolysis. The Hemolytic Index (HI = HC50/MIC) for F3 against *S. aureus* was 8.0 (500/62.5). As noted in Methods, no universally accepted HI threshold exists; the bands (HI > 10, wide margin; HI 5–10, intermediate margin) are used here only for relative comparison and not as a regulatory acceptance criterion. Absolute safety for food use must be established by challenge testing and toxicological assessment. F1, with virtually no hemolytic activity (HC_{50} >1000 µg/mL), was classified as non-hemolytic, consistent with its weak antimicrobial activity. The hemolytic profile of F3 paralleled its MTT cytotoxicity data (IC_{50} = 350 µg/mL), with the HC_{50} approximately 1.4-fold higher than the MTT IC_{50}, suggesting somewhat greater selectivity for bacterial over mammalian erythrocyte membranes.

3.7 Cytotoxicity and Selectivity Index

MTT assays confirmed favorable safety profiles (Figure 4; Supplementary Tables 3–5). At 100 µg/mL, cell viability in MCF-7 cells was 77.9 ± 3.2% (Alcalase), 81.4 ± 2.8% (papain), and 88.6 ± 2.5% (trypsin). IC_{50} values were 350 µg/mL (95% CI: 328–374) for Alcalase, 420 µg/mL (CI: 392–451) for papain, and >500 µg/mL for trypsin. HepG2 IC_{50} values were 405, 495, and 560

View Article Online
DOI: 10.1039/D6FB00050A

µg/mL, respectively. The SI for Alcalase hydrolysate against *S. aureus* was 5.6 (MCF-7) and 6.5 (HepG2). The combined safety profile—SI of 5.6 from cytotoxicity data and HI of 8.0 from hemolysis—provides convergent evidence of an adequate safety window for food preservation applications.

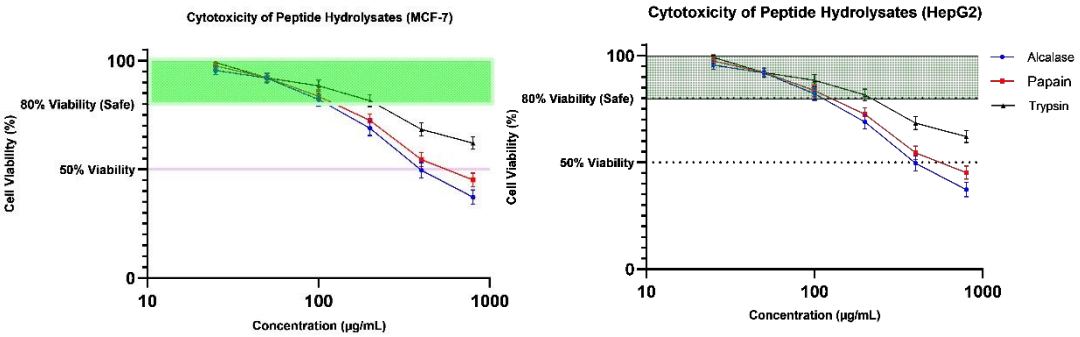

Figure 4. *MTT-based cell viability of* ***(A) MCF-7*** *and* ***(B) HepG2*** *cells after 48 h exposure to crude hydrolysates prepared with Alcalase, papain, or trypsin at concentrations of* ***25****–800 µg/mL. Data are presented as mean ± SD from three independent experiments (n =* ***3****). The shaded region above 80% viability indicates a commonly applied reference range for preliminary cytocompatibility screening, and the dotted line at 50% viability indicates the approximate* IC_{50} *threshold. Doxorubicin (10 µM) was used as a cytotoxic positive control, but it is not shown on the hydrolysate dose–response curves because it was tested at a single concentration in a different unit system. Statistical comparisons among hydrolysates at each concentration were performed by one-way ANOVA followed by Tukey's post-hoc test, and significance, where present, is indicated in the figure. Because both cell models are transformed cell lines, these results are interpreted as a preliminary cytocompatibility screen rather than definitive safety evidence.*

3.8 Multi-Assay Antioxidant Capacity

3.8.1 DPPH Radical Scavenging

F3 exhibited the strongest DPPH activity (IC_{50} = 0.62 ± 0.04 mg/mL; 95% CI: 0.58–0.67), approximately 2.3-fold more potent than the crude hydrolysate (IC_{50} = 1.85 ± 0.12 mg/mL) and 2.2–4.4-fold more potent than other fractions. F2 and F4 showed similar intermediate activity (IC_{50} = 1.42 ± 0.09 and 1.38 ± 0.10 mg/mL; $p > 0.05$). F1 was weakest (IC_{50} = 2.75 mg/mL). Trolox IC_{50} = 0.018 mg/mL (Supplementary Table 6).

3.8.2 ABTS Radical Scavenging

View Article Online
DOI: 10.1039/D6FB00050A

The ABTS assay confirmed the DPPH pattern (Table 5). F3 showed IC_{50} = 0.89 ± 0.06 mg/mL, significantly more potent than F2 (1.68 ± 0.11), F4 (1.52 ± 0.09), and F1 (3.12 ± 0.18 mg/mL; all $p < 0.001$). The identical rank order across both radical scavenging assays (F3 > F4 ≈ F2 > F1) provided convergent evidence. The Trolox positive control, run in parallel, is reported in Table 5 for reference.

3.8.3 FRAP

FRAP analysis yielded the same hierarchy (Table 5). F3 gave 142.5 ± 8.9 µmol TE/g, significantly exceeding F2 (95.7 ± 6.8), F4 (88.2 ± 5.6), and F1 (48.3 ± 4.2; all $p < 0.001$). The consistent superiority of F3 across three mechanistically distinct assays—electron transfer (DPPH), mixed-mechanism scavenging (ABTS), and metal reduction (FRAP)—constitutes robust evidence for genuine antioxidant capacity in the 1–3 kDa range.

Table 5: Antioxidant activity of peptide fractions: ABTS radical-scavenging IC_{50} and FRAP, with Trolox positive control. Values are mean±SD

Sample	ABTS IC50 (mg/mL)	FRAP (µmol TE/g)
F1 (>10 kDa)	3.12 ± 0.18	48.3 ± 4.2
F2 (3–10 kDa)	1.68 ± 0.11	95.7 ± 6.8
F3 (1–3 kDa)	0.89 ± 0.06	142.5 ± 8.9
F4 (<1 kDa)	1.52 ± 0.09	88.2 ± 5.6
Trolox (positive control)	0.012	reference standard (TE basis)

4. DISCUSSION

4.1 Enzyme Selection and Process Optimization

The finding that Alcalase outperformed both papain and trypsin in hydrolytic efficiency is consistent with its established broad specificity and alkaline stability, and aligns with reports from other plant protein substrates including soy (Islam et al., 2022), rapeseed (He et al., 2013), and pea (Gan et al., 2025). The DH of 59.9% compares favorably with these systems, indicating efficient protein mobilization from the Moringa leaf matrix. The strong correlation between DH ranking and bioactivity ranking supports the view that Alcalase generates a more diverse and functionally favorable peptide population, likely because its preference for hydrophobic cleavage sites yields

View Article Online
DOI: 10.1039/D6FB00050A

peptides with terminal hydrophobic residues—a feature associated with enhanced membrane interaction and radical scavenging.

4.2 Structural Validation

The use of Tricine-SDS-PAGE was essential for resolving peptides in the bioactively relevant 1–10 kDa range, where standard Laemmli gels offer no useful resolution (Rabilloud & Lelong, 2011; Schägger, 2006). FTIR data complemented the electrophoretic evidence by demonstrating that peptide bond integrity was maintained throughout purification. The persistence of the Amide I band at 1635–1640 cm^{-1} rules out the possibility that observed bioactivities arise from free amino acids or non-peptidic contaminants. The progressive spectral attenuation in smaller fractions is consistent with shorter chains possessing less ordered secondary structure (Nirmal et al., 2024; Oberg et al., 2004).

4.3 Size–Activity Relationships and Structural Rationale

The bell-shaped dependence of both antimicrobial and antioxidant activity on molecular weight, with a clear optimum at 1–3 kDa, is among the most informative findings of this study. Peptides in this range (~10–27 residues) occupy a functional sweet spot: sufficient length to support amphipathic organization yet short and flexible enough for membrane insertion and disruption (Jenssen et al., 2006; Yeaman & Yount, 2003). The steep decline for F1 (>10 kDa; 15.2% inhibition) likely reflects stable tertiary folds that bury hydrophobic surfaces, while F4's intermediate activity (52.6%) suggests a threshold length requirement for effective membrane contact.

Compositional analysis supported this interpretation. Among all fractions, F3 exhibited the most favorable balance of hydrophobic content (45%) and cationic density (0.15 residues/aa)—closely matching the compositional requirements established for potent antimicrobial peptides (40–60% hydrophobic; net positive charge; (Brogden, 2005; Haney et al., 2019). The hydrophobic–cationic composite index correlated strongly with antimicrobial potency ($R^2 = 0.87$; Supplementary Figure 3), consistent with models requiring coordinated hydrophobic insertion and electrostatic membrane attraction (Talapko et al., 2022).

The exploratory AlphaFold2 predictions offer a structural perspective on these compositional observations. The predicted conformational flexibility and spatial segregation of hydrophobic and

View Article Online
DOI: 10.1039/D6FB00050A

polar residues in representative F3-sized peptides are consistent with the canonical mechanism of antimicrobial peptide action: electrostatic attraction to anionic bacterial membranes, followed by hydrophobic insertion and membrane destabilization (Wimley & Hristova, 2011; Zasloff, 2002). While these computational predictions must be interpreted with appropriate caution given the known limitations of AlphaFold2 for short, flexible peptides(McDonald et al., 2023), they provide a plausible structural framework for the observed size–activity pattern and generate testable hypotheses for future biophysical characterization through circular dichroism and NMR studies.

4.4 Multi-Assay Antioxidant Validation

The use of three mechanistically distinct antioxidant assays addresses the well-documented limitation that single-assay characterization is prone to mechanism-specific artifacts (Rumpf et al., 2023; Xiao et al., 2020). The identical rank order of fractions across DPPH, ABTS, and FRAP provides strong evidence that F3's antioxidant capacity is genuine. The co-localization of maximal antimicrobial and antioxidant activities in F3 is mechanistically coherent: while membrane-active antimicrobial function depends on amphipathic topology, radical scavenging derives from electron-donating aromatic and sulfur-containing residues (Sarmadi & Ismail, 2010; Udenigwe & Aluko, 2012). The 1–3 kDa size range appears optimal for accommodating both types of functional motif simultaneously (Power et al., 2013).

4.5 Safety Assessment: Convergent Evidence from Hemolysis and Cytotoxicity

A distinguishing feature of this study is the dual safety assessment combining conventional MTT cytotoxicity with erythrocyte hemolysis. The Hemolytic Index of 8.0 for F3 (HC_{50} = 500 μg/mL; MIC = 62.5 μg/mL) and the Selectivity Index of 5.6 (IC_{50} = 350 μg/mL; MIC = 62.5 μg/mL) provide convergent evidence of an adequate safety margin for food preservation applications. The HI of 8.0 for F3 indicates that the antibacterial MIC is reached at roughly one-eighth of the HC50, a comparatively wide margin that is consistent with preferential disruption of bacterial over mammalian membranes; we interpret this value relatively rather than against any fixed regulatory threshold (Zhang et al., 2021). This selectivity likely reflects differences in membrane composition: bacterial membranes are enriched in anionic phospholipids (phosphatidylglycerol, cardiolipin) that attract cationic peptides, whereas mammalian erythrocyte membranes contain predominantly zwitterionic phospholipids (phosphatidylcholine,

View Article Online
DOI: 10.1039/D6FB00050A

sphingomyelin) that present a less favorable electrostatic surface for peptide binding (Wimley & Hristova, 2011).

The finding that HC_{50} exceeded IC_{50} (MTT) by approximately 1.4-fold suggests that erythrocytes are somewhat more resistant to the peptide fraction than proliferating tumor cell lines, possibly owing to the non-proliferative, highly elastic nature of the red blood cell membrane. For food applications, where the peptide fraction would be applied at concentrations near the MIC (62.5–125 μg/mL), hemolysis would remain below 12%, well within acceptable limits for food-grade ingredients.

4.6 Dual Functionality for Food Preservation

The co-localization of antimicrobial and antioxidant activities in a single fraction offers practical advantages for food preservation, where microbial spoilage and oxidative degradation are the two primary shelf-life limiting mechanisms (Talapko et al., 2022). F3's MIC values (62.5–125 μg/mL) compare favorably with other plant-derived peptide hydrolysates: pea peptides (MIC 100–250 μg/mL; (Gan et al., 2025), soy peptides (MIC 125–350 μg/mL; (Islam et al., 2022), and Moringa leaf peptides characterized by (Wang et al., 2025). Potential applications include edible coatings for fresh produce, preservatives for minimally processed meats, and natural antioxidant additives for oil-based systems (Nirmal et al., 2024). The use of a widely cultivated, fast-growing tropical species as the protein source, combined with a simple enzyme-plus-ultrafiltration workflow that requires no organic solvents or chromatographic steps, positions this approach as both economically accessible and environmentally sustainable (supplementary table S8). Importantly, because all processing steps employ food-grade reagents and equipment already available in small-to-medium food enterprises, scale-up to pilot production is technically straightforward, making this technology particularly relevant for food manufacturers in tropical and subtropical regions where M. oleifera is abundantly available and synthetic preservatives remain costly or poorly regulated.

4.7 Limitations and Future Directions

Several aspects of this work merit further development. The peptide fractions were characterized at the mixture level; LC-MS/MS-based sequence identification would reveal the molecular identities of the active species within F3 and enable structure–activity analysis at the individual peptide level. The in silico structural predictions, while informative, were based on

View Article Online
DOI: 10.1039/D6FB00050A

computationally derived sequences rather than experimentally confirmed ones, and AlphaFold2's reliability diminishes for short, flexible peptides (McDonald et al., 2023); circular dichroism and NMR spectroscopy applied to experimentally identified sequences would yield definitive conformational data. The antimicrobial spectrum should be expanded to include additional food-relevant pathogens and drug-resistant strains, ideally accompanied by time-kill kinetics and membrane permeabilization assays (NPN uptake, SYTOX Green) to establish the mechanism of action. Finally, stability testing under simulated food processing conditions (thermal stress, pH extremes, gastrointestinal digestion) will be essential to translate these findings into practical preservative applications. Challenge tests in model food systems—such as inoculated fresh-cut fruit, ground meat, and emulsion-based dressings—should be prioritized to validate shelf-life extension under realistic storage conditions. Sensory evaluation will also be necessary to confirm that incorporation of the peptide fraction at effective concentrations does not adversely affect taste, color, or texture of the final food product.

5. CONCLUSION

This work shows that Moringa oleifera leaf protein can be converted, using a simple food-grade enzymatic process, into peptide fractions that combine relevant antimicrobial and antioxidant activities with a favourable in vitro safety profile. Among the tested fractions, the 1–3 kDa pool (F3) consistently performed best across all assays, supporting it as a rational candidate for further development as a dual-function preservative. Because the production pipeline relies only on Alcalase hydrolysis and membrane ultrafiltration, without organic solvents or specialized equipment, it is in principle compatible with scale-up in typical food and ingredient processing settings. We emphasise, however, that the present evidence rests on in vitro assays of unsequenced peptide mixtures; identification of the active peptides by LC-MS/MS, together with stability and challenge testing in representative food matrices, is required before specific preservative or clean-label applications can be claimed. These steps, alongside sensory evaluation, define the priorities for future work.

CONFLICT OF INTEREST

The authors declare no conflict of interest.

View Article Online
DOI: 10.1039/D6FB00050A

DATA AVAILABILITY

Data supporting these findings are available from the corresponding author upon reasonable request.

ACKNOWLEDGMENTS

The authors thank the University of Sulaimani and Komar University of Science and Technology for laboratory facilities.

References

Bahar, A. A., & Ren, D. (2013). Antimicrobial peptides. In *Pharmaceuticals* (Vol. 6, Number 12, pp. 1543–1575). MDPI AG. https://doi.org/10.3390/ph6121543

Brogden, K. A. (2005). Antimicrobial peptides: Pore formers or metabolic inhibitors in bacteria? In *Nature Reviews Microbiology* (Vol. 3, Number 3, pp. 238–250). https://doi.org/10.1038/nrmicro1098

Chalamaiah, M., Yu, W., & Wu, J. (2018). Immunomodulatory and anticancer protein hydrolysates (peptides) from food proteins: A review. In *Food Chemistry* (Vol. 245, pp. 205–222). Elsevier Ltd. https://doi.org/10.1016/j.foodchem.2017.10.087

Craik, D. J., Fairlie, D. P., Liras, S., & Price, D. (2013). The Future of Peptide-based Drugs. *Chemical Biology and Drug Design*, *81*(1), 136–147. https://doi.org/10.1111/cbdd.12055

Gan, Y., Xie, N., & Zhang, D. (2025). Pea-Derived Antioxidant Peptides: Applications, Bioactivities, and Mechanisms in Oxidative Stress Management. In *Chemistry (Switzerland)* (Vol. 7, Number 5). Multidisciplinary Digital Publishing Institute (MDPI). https://doi.org/10.3390/chemistry7050141

Gopalakrishnan, L., Doriya, K., & Kumar, D. S. (2016). Moringa oleifera: A review on nutritive importance and its medicinal application. In *Food Science and Human Wellness* (Vol. 5, Number 2, pp. 49–56). Elsevier B.V. https://doi.org/10.1016/j.fshw.2016.04.001

Haney, E. F., Straus, S. K., & Hancock, R. E. W. (2019). Reassessing the host defense peptide landscape. In *Frontiers in Chemistry* (Vol. 7, Number FEB). Frontiers Media S.A. https://doi.org/10.3389/fchem.2019.00043

He, R., Girgih, A. T., Malomo, S. A., Ju, X., & Aluko, R. E. (2013). Antioxidant activities of enzymatic rapeseed protein hydrolysates and the membrane ultrafiltration fractions. *Journal of Functional Foods*, *5*(1), 219–227. https://doi.org/10.1016/j.jff.2012.10.008

Huang, Z., Dong, W., Zou, L., Zhao, Q., Tian, Y., Huang, A., & Wang, X. (2024). Study of the antibacterial properties of antimicrobial peptide MOp2 from Moringa oleifera seeds against S. aureus through transcriptomic techniques. *LWT*, *191*. https://doi.org/10.1016/j.lwt.2023.115636

Islam, M., Huang, Y., Islam, S., Fan, B., Tong, L., & Wang, F. (2022). Influence of the Degree of Hydrolysis on Functional Properties and Antioxidant Activity of Enzymatic Soybean Protein Hydrolysates. *Molecules*, *27*(18). https://doi.org/10.3390/molecules27186110

View Article Online
DOI: 10.1039/D6FB00050A

Jenssen, H., Hamill, P., & Hancock, R. E. W. (2006). Peptide antimicrobial agents. In *Clinical Microbiology Reviews* (Vol. 19, Number 3, pp. 491–511). https://doi.org/10.1128/CMR.00056-05

McDonald, E. F., Jones, T., Plate, L., Meiler, J., & Gulsevin, A. (2023). Benchmarking AlphaFold2 on peptide structure prediction. *Structure*, *31*(1), 111-119.e2. https://doi.org/10.1016/j.str.2022.11.012

Nirmal, N., Khanashyam, A. C., Shah, K., Awasti, N., Sajith Babu, K., Ucak, İ., Afreen, M., Hassoun, A., & Tuanthong, A. (2024). Plant protein-derived peptides: frontiers in sustainable food system and applications. In *Frontiers in Sustainable Food Systems* (Vol. 8). Frontiers Media SA. https://doi.org/10.3389/fsufs.2024.1292297

Oberg, K. A., Ruysschaert, J. M., & Goormaghtigh, E. (2004). The optimization of protein secondary structure determination with infrared and circular dichroism spectra. *European Journal of Biochemistry*, *271*(14), 2937–2948. https://doi.org/10.1111/j.1432-1033.2004.04220.x

Parvez, A. K., Jubyda, F. T., Ayaz, M., Sarker, A., Haque, N., Khan, M. S., Mou, T. J., Rahman, M. A., & Huq, M. A. (2024). Microbial- and Plant-Derived Bioactive Peptides and Their Applications against Foodborne Pathogens: Current Status and Future Prospects. In *International Journal of Microbiology* (Vol. 2024). Hindawi Limited. https://doi.org/10.1155/2024/9978033

Power, O., Jakeman, P., & Fitzgerald, R. J. (2013). Antioxidative peptides: Enzymatic production, in vitro and in vivo antioxidant activity and potential applications of milk-derived antioxidative peptides. In *Amino Acids* (Vol. 44, Number 3, pp. 797–820). https://doi.org/10.1007/s00726-012-1393-9

Rabilloud, T., & Lelong, C. (2011). Two-dimensional gel electrophoresis in proteomics: A tutorial. In *Journal of Proteomics* (Vol. 74, Number 10, pp. 1829–1841). https://doi.org/10.1016/j.jprot.2011.05.040

Rivero-Pino, F., Leon, M. J., Millan-Linares, M. C., & Montserrat-de la Paz, S. (2023). Antimicrobial plant-derived peptides obtained by enzymatic hydrolysis and fermentation as components to improve current food systems. In *Trends in Food Science and Technology* (Vol. 135, pp. 32–42). Elsevier Ltd. https://doi.org/10.1016/j.tifs.2023.03.005

Rumpf, J., Burger, R., & Schulze, M. (2023). Statistical evaluation of DPPH, ABTS, FRAP, and Folin-Ciocalteu assays to assess the antioxidant capacity of lignins. *International Journal of Biological Macromolecules*, *233*. https://doi.org/10.1016/j.ijbiomac.2023.123470

Sarmadi, B. H., & Ismail, A. (2010). Antioxidative peptides from food proteins: A review. In *Peptides* (Vol. 31, Number 10, pp. 1949–1956). https://doi.org/10.1016/j.peptides.2010.06.020

Schägger, H. (2006). Tricine-SDS-PAGE. *Nature Protocols*, *1*(1), 16–22. https://doi.org/10.1038/nprot.2006.4

Talapko, J., Meštrović, T., Juzbašić, M., Tomas, M., Erić, S., Horvat Aleksijević, L., Bekić, S., Schwarz, D., Matić, S., Neuberg, M., & Škrlec, I. (2022). Antimicrobial Peptides—Mechanisms of Action, Antimicrobial Effects and Clinical Applications. In *Antibiotics* (Vol. 11, Number 10). MDPI. https://doi.org/10.3390/antibiotics11101417

Udenigwe, C. C., & Aluko, R. E. (2012). Food protein-derived bioactive peptides: Production, processing, and potential health benefits. In *Journal of Food Science* (Vol. 77, Number 1). https://doi.org/10.1111/j.1750-3841.2011.02455.x

View Article Online
DOI: 10.1039/D6FB00050A

Wang, J., Yang, T., Yu, W., Zhou, J., Bian, Y., Li, S., & Chen, Y. (2025). Pea power against microbes: Elucidating the characteristics and antimicrobial mechanisms of antimicrobial peptides obtained through enzymatic hydrolysis of pea protein isolate. *Food Bioscience*, *65*, 106075. https://doi.org/10.1016/j.fbio.2025.106075

Wiegand, I., Hilpert, K., & Hancock, R. E. W. (2008). Agar and broth dilution methods to determine the minimal inhibitory concentration (MIC) of antimicrobial substances. *Nature Protocols*, *3*(2), 163–175. https://doi.org/10.1038/nprot.2007.521

Wimley, W. C., & Hristova, K. (2011). Antimicrobial peptides: Successes, challenges and unanswered questions. *Journal of Membrane Biology*, *239*(1–2), 27–34. https://doi.org/10.1007/s00232-011-9343-0

Xiao, F., Xu, T., Lu, B., & Liu, R. (2020). Guidelines for antioxidant assays for food components. In *Food Frontiers* (Vol. 1, Number 1, pp. 60–69). John Wiley and Sons Inc. https://doi.org/10.1002/fft2.10

Yeaman, M. R., & Yount, N. Y. (2003). Mechanisms of antimicrobial peptide action and resistance. In *Pharmacological Reviews* (Vol. 55, Number 1, pp. 27–55). https://doi.org/10.1124/pr.55.1.2

Zasloff, M. (2002). Antimicrobial peptides of multicellular organisms. In *NATURE* | (Vol. 415). www.nature.com

Zhang, Q. Y., Yan, Z. Bin, Meng, Y. M., Hong, X. Y., Shao, G., Ma, J. J., Cheng, X. R., Liu, J., Kang, J., & Fu, C. Y. (2021). Antimicrobial peptides: mechanism of action, activity and clinical potential. In *Military Medical Research* (Vol. 8, Number 1). BioMed Central Ltd. https://doi.org/10.1186/s40779-021-00343-2

Zhao, Q., He, L., Wang, X., Ding, X., Li, L., Tian, Y., & Huang, A. (2022). Characterization of a Novel Antimicrobial Peptide Isolated from *Moringa oleifera* Seed Protein Hydrolysates and Its Membrane Damaging Effects on *Staphylococcus aureus*. *Journal of Agricultural and Food Chemistry*, *70*(20), 6123–6133. https://doi.org/10.1021/acs.jafc.2c01335

View Article Online
DOI: 10.1039/D6FB00050A

Data Availability Statement:

Data supporting these findings are available from the corresponding author upon reasonable request.